

Growth control of peptide-nanotube spherulitic films: Experiments and simulations

Netta Hendler^{1,2}, Elad Mentovich^{1,2}, Bálint Korbuly³, Tamás Pusztai³, László Gránásy^{3,4} (✉),
Shachar Richter^{1,2} (✉)

¹ Department of Materials Science and Engineering, Faculty of Engineering, Tel Aviv University, Ramat Aviv, Tel Aviv 69978, Israel

² Center for Nanoscience and Nanotechnology, Tel Aviv University, Ramat Aviv, Tel Aviv 69978, Israel

³ Wigner Research Centre for Physics, P.O. Box 49, H-1525 Budapest, Hungary

⁴ Brunel Centre for Advanced Solidification Technology, Brunel University, Uxbridge, Middlesex, UB8 3PH, UK

Received: 6 January 2015

Revised: 11 June 2015

Accepted: 17 July 2015

© Tsinghua University Press
and Springer-Verlag Berlin
Heidelberg 2015

KEYWORDS

multi-hierarchical
self-assembly,
growth-front nucleation,
peptide nanotubes,
spherulite,
crystallization,
experiment vs.
phase-field modeling

ABSTRACT

Multi-hierarchical self-assembly (MHSA) is a key process responsible for the spontaneous formation of many complex structures. However, because of the complexity of the process, the underlying mechanism remains largely unclear. Thus, a deeper understanding of MHSA is required, especially for the preparation of MHSA systems via bottom-up methodologies. We show here, experimentally and theoretically, that the complex-formation MHSA of peptide nanotube films can be controlled solely by manipulating the experimental parameter of humidity. Furthermore, we identify growth-front nucleation (GFN; the formation of new grains at the perimeter) as the physical background for the observed morphological transitions by correlating experimental observations with phase-field modeling of the morphological evolution. Our findings indicate a simple way to control multi-hierarchical morphologies, crucial for the employment of bottom-up techniques in constructing complex structures for practical applications.

1 Introduction

Multi-hierarchical self-assembly (MHSA) is responsible for the spontaneous formation of many complex structures [1] including the crystalline aggregation of gold-DNA nanoparticles [2], self-arrangement of carbon nanotubes [3], and protein self-assembly [4, 5]. However,

in most systems, the mechanism of MHSA has been deduced from individual case studies [6]; these have not yet been condensed into general principles.

One of the most extensively studied systems displaying MHSA is peptide-based nanotubes (PNTs) in solution. A variety of techniques has been developed to achieve MHSA with PNTs [6, 8, 9]. PNT films also

Address correspondence to Shachar Richter, srichter@post.tau.ac.il; László Gránásy, granasy.laszlo@wigner.mta.hu

display promising properties for electronic [7], microfluidic, and optical applications [6, 9].

We, among others, have extensively characterized PNTs in previous reports [8–10] and developed an MHSAs process to form ordered arrays of PNT films via a simple bottom-up approach. The method includes the dissociation of the PNTs in a polar cosolvent solution and deposition of the tubes on solid substrates, resulting in long-range MHSAs among the PNTs [8].

Other attempts have included the large-scale assembly of PNTs in spherulitic films utilizing complex evaporation techniques [6] and the horizontal alignment of PNTs through the application of a non-covalent ferrofluidic coating followed by exposure to an external magnetic field [9]. We have observed a broad range of spherulitic morphologies in PNT thin films, shown in the first row of Fig. 1. Previous work [8–10] has indicated that such spherulites are indeed built of PNTs. This is clear from the comparison of X-ray diffraction data for the spherulites with that for samples known to be composed of PNTs, and is supported by atomic force microscopy results in the Electronic Supplementary

Material (ESM). Furthermore, different types of PNTs can form spherulites (see Ref. [10]). Although the formation mechanism of PNT spherulites remains under the subject of further investigation, it is suspected to be universal.

Spherulites are micron-scale polycrystalline growth forms ubiquitous under highly non-equilibrium conditions [11]. They have been observed in many materials, including pure Se [12], oxide and metallic glasses [13, 14], minerals, volcanic rocks, polymers [11, 15], liquid crystals [16], and organic materials [17]. The term “spherulite” is often used in a broader sense to denote densely branched partly or fully crystalline objects of roughly spherical envelopes (circular in two dimensions). They are classified into two main categories: Category 1 spherulites grow radially from the nucleation site, branching intermittently to maintain a space-filling character. By contrast, Category 2 spherulites form via branching at the two ends of the initial needle crystal formed by nucleation, which process yields a crystal “sheaf” that spreads increasingly during growth. With further growth, these sheaves

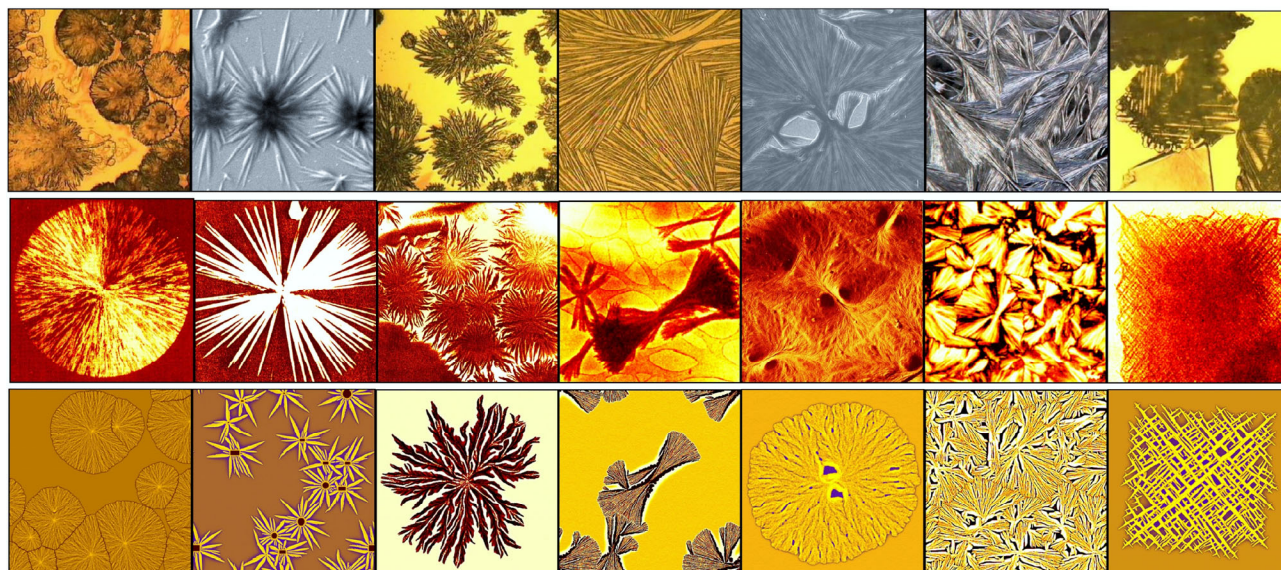


Figure 1 Polycrystalline growth morphologies formed by multi-hierarchy self-assembly of PNTs (this work, upper row), in Se (reproduced with permission from Ref. [12], © Elsevier 1988) and polymeric materials (reproduced with permission from Ref. [17], © American Institute of Physics 1966; presented by the courtesy of Walker et al. [18]; reproduced with permission from Ref. [19], © American Chemical Society 1993; reproduced with permission from Ref. [20], © Wiley 1963; reproduced with permission from Ref. [21], © American Chemical Society 2000; and reproduced with permission from [22], © The National Institute of Standards and Technology (NIST) 1996) (central row), and in phase-field simulations (reproduced from Ref. [24], © American Physical Society 2005) (bottom row). Note the close similarity of the solidification forms in systems of very different molecular properties. From left to right, the sequence of the morphologies is as follows: Category 1 spherulites, spiky forms, “cabbages”, sheaves, Category 2 spherulites with the “eyes”, overlapping sheaves, and “quadrates”.

develop two “eyes” of uncrystallized material on each side of the nucleation site. Ultimately, this type of the spherulite develops a roughly spherical growth pattern, with eye structures apparent in the core region. Representative examples of spherulitic patterns found in various experimental systems [12, 17–22] are shown in the second row of Fig. 1.

Materials of substantially different molecular geometry (e.g., oxide glass, uric acid, graphite, insulin, and PNTs) form very similar spherulites, suggesting that a coarse-grained description that neglects molecular details could feasibly describe spherulitic solidification. Indeed, recent simulations based on phase-field theory [23, 24], which relies on coarse-grained-order parameter fields and thus neglects molecular details, yield growth morphologies very similar to experimental examples (see third row of Fig. 1) [24].

Here, we compare crystal-growth experiments on PNTs with phase-field simulations. Relying on the observed similarities between the experimental and simulated results, we propose the previously identified phenomenon of growth-front nucleation (GFN) as a new paradigm for bottom-up synthesis approaches, based on the MHSA of spherulitic PNTs. Furthermore, we identify this MHSA system as a new test bed for the polycrystalline growth puzzle, as we successfully control spherulitic growth via tuning the single parameter of humidity. The identification of this control mechanism in the present work may permit the mathematical modeling of the MHSA process, which should incorporate the following aspects: (1) water adsorption on the sample surface, (2) water transport inside the sample, and (3) computation of the effect of the local water content on the thermodynamic driving force of crystallization, which are coupled finally to (4) the phase-field modeling of spherulite formation. Such modeling support is expected to improve the quality and reproducibility of experimental samples, and may facilitate the optimization of the materials properties of spherulites for application.

2 Results and discussion

2.1 Preparation of PNT films

PNTs (Bachem, Switzerland) were diluted with

10% (*v/v*) N-methyl-2-pyrrolidone (NMP) (Ashland Chemical) and sonicated for 5 min. The solution was then incubated overnight at room temperature, deposited on a preheated surface (60 °C) located in a controlled-humidity chamber, until complete evaporation of the solvent. The resulting PNT films exhibit unique spherulitic forms (Fig. 1). Our observations indicate that the morphology formed by self-assembly of PNTs as well as the average surface coverage correlates strongly with humidity. A quantitative example is shown in Fig. 2. At low humidity, the PNTs form needle-like crystals (Fig. 2, 50% humidity). With increasing humidity, they are replaced by axialites (Fig. 2, 60% humidity), then by crystal sheaves (Fig. 2, 65% humidity), and finally Category 2 spherulites

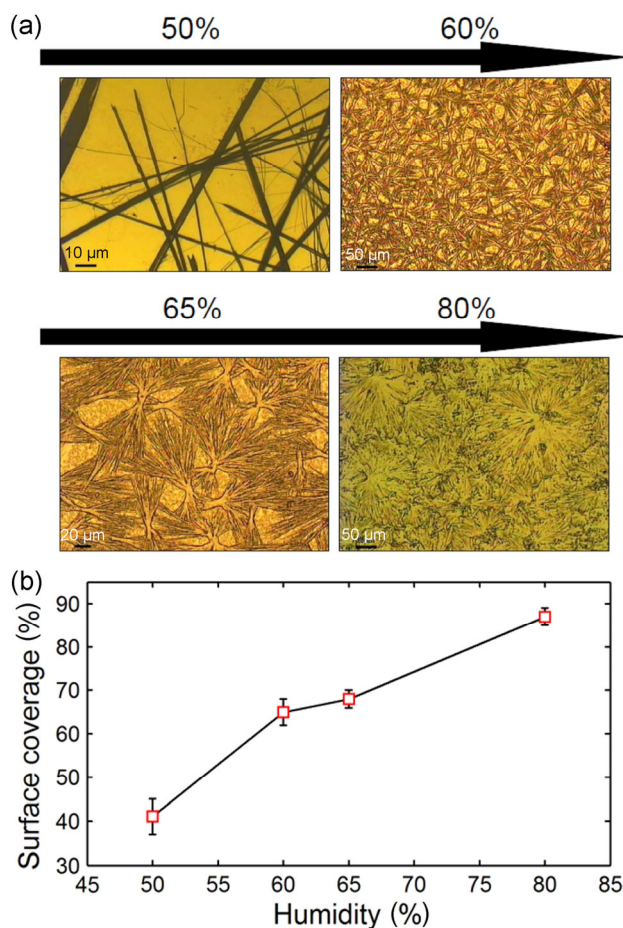


Figure 2 The effect of humidity on crystal growth of PNT aggregates on alumina substrate. (a) Morphology vs. humidity. Scale bars: 50%, 10 μm; 60%, 50 μm; 65%, 20 μm; and 80%, 50 μm. The sequence of morphologies ranges from a multiplicity of needle-shaped crystals to polycrystalline sheaves and finally to spherulites. (b) Surface coverage vs. humidity.

appear (Fig. 2, 80% humidity). Furthermore, it is found that elevated humidity diminishes the “eyes” of Category 2 spherulites, as also observed in our phase-field simulations when the supersaturation (driving force) is increased [24]. (For growth results under different conditions see the ESM.)

Similar morphological transitions are also observed on a quartz substrate (Fig. 3). While the humidity values for the morphological changes differ from those observed for the spherulites grown on alumina, the sequence of solidification morphologies remains the same.

2.2 Phase-field results

We recall next some relevant predictions of the phase-field theory [23, 24]. It has been shown that polycrystalline growth leading to spherulitic solidification arises either from quenching orientational defects (interpreted as dislocation groups) into the solid, which may arise from (i) static heterogeneities (impurities) [23] or (ii) dynamic heterogeneities intrinsic to supercooled liquids [23], or from (iii) branching of the crystal with a fixed crystallographic misorientation [24]. These processes of creating new crystal grains at the perimeter of the growing crystal are examples of growth-front nucleation (GFN).

Mechanism (i) is a heterogeneous mode of GFN in which the interaction of foreign particles with the growth front leads to the formation of new grains, whereas (ii) and (iii) are considered homogeneous modes of GFN. The three modes of GFN yield strikingly similar crystallization morphologies [23, 24].

Accordingly, spherulite formation is expected to occur in highly impure or highly supercooled fluids as well as in systems in which low-energy grain boundaries are available for branching. Here we focus on the homogeneous modes of GFN. A model incorporating mechanisms (ii) and (iii) provides a general description of polycrystalline solidification that suitably describes the evolution of complex polycrystalline spherulites, as demonstrated earlier [23, 24]. While mechanism (ii) is expected when the ratio χ of the rotational and translational diffusion coefficients, $\chi = D_{\text{rot}}/D_{\text{trans}}$, is sufficiently low due to molecular geometry or specifically “decoupling” in the neighborhood of the glass transition temperature [23], whereas mechanism (iii) is expected for small degrees of undercooling [24], where χ is constant.

In the phase-field modeling of spherulites in two dimensions, we rely on a general model of polycrystalline solidification, as described in Refs. [23, 24], which builds on the phase-field models of the primary nucleation and growth of crystals from the melt [25] and multigrain solidification [26–28]. In addition to the diffusional instabilities and anisotropies of the interface free energy and molecule-attachment kinetics, the model includes mechanisms (ii) and (iii) to incorporate orientational defects into the solid. The local state of matter is characterized by a coarse-grained-order parameter, the phase field ϕ , that monitors the structural change during solidification. Other coarse-grained-field variables include the chemical composition field c and the scalar orientation field θ . The latter specifies the orientation of crystal planes in

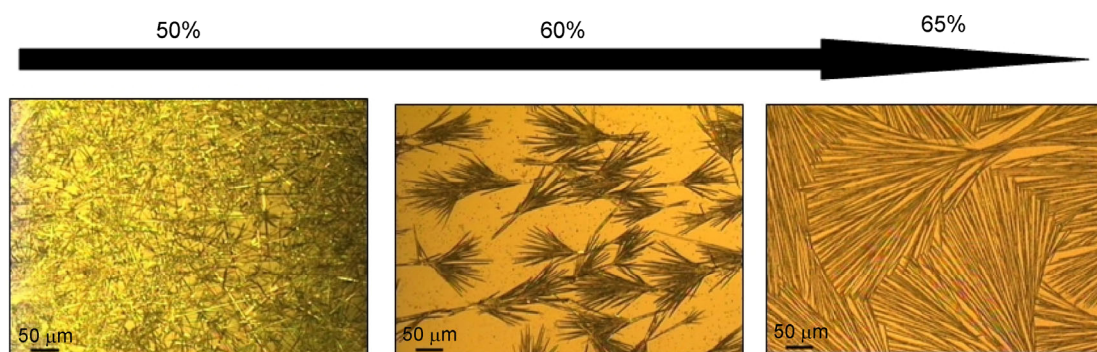


Figure 3 The effect of humidity on the growth morphology of PNT on a quartz substrate. The sequence of morphologies, ranging from a multiplicity of needle crystals to polycrystalline sheaves to spherulites, suggests that the results shown in Figs. 2 and 3 are independent of the substrate. Scale bar for all images: 50 μm .

the laboratory frame. The free energy F is defined as

$$F = \int dr \left\{ \frac{\alpha^2 T}{2} |\nabla \phi|^2 + f(\phi, c, T) + f_{\text{ori}}(\phi, |\nabla \theta|) \right\} \quad (1)$$

where α is a constant, T the temperature, $f(\phi, c, T)$ the free-energy density, and f_{ori} the orientational contribution to F . The gradient term for the phase field generates a diffuse crystal-liquid interface, observed both experimentally and in computer simulations. The free-energy density $f(\phi, c, T)$ has two minima ($\phi = 0$ and $\phi = 1$), which correspond to the crystalline and liquid phases. The relative depth of these minima is the driving force for crystallization and changes with both temperature and composition [23, 24].

The time evolutions of the phase and orientation fields are described by non-conservative equations of motion (EOMs), whereas an EOM that realizes conservative dynamics is used to describe that of the concentration field as follows

$$\begin{aligned} \dot{\phi} &= -M_{\phi} \left(\frac{\delta F}{\delta \phi} \right) + \zeta_{\phi} \\ \dot{c} &= \nabla \cdot \left[M_c \nabla \left(\frac{\delta F}{\delta c} \right) + \zeta_j \right] \\ \dot{\theta} &= -M_{\theta} \left(\frac{\delta F}{\delta \theta} \right) + \zeta_{\theta} \end{aligned} \quad (2)$$

where $(\delta F/\delta X)$ denotes the functional derivative of the free energy with respect to field X (where $X = \phi, c,$ or θ), and M_{ϕ} , M_c , and M_{θ} represent the mobilities setting the time scales of their respective fields in proportion to the translational, chemical, and rotational diffusion coefficients. The thermal fluctuations are represented by noise terms ζ_{ϕ} , ζ_j , and ζ_{θ} added to the EOMs. In the case of the concentration field a flux noise (ζ_j) applies, as opposed to the additive noise of the non-conserved fields (ζ_{ϕ} and ζ_{θ}) [23, 24]. The EOMs have been solved numerically by a finite difference discretization and an Euler forward-stepping scheme, implemented in a massively parallel environment (see Ref. [24]).

Based on previous work on the phase-field modeling of spherulite formation [23, 24], the governing parameters that can be used to control the intensity of GFN, corresponding to the propensity for spherulite

formation, are (a) the thermodynamic driving force of crystallization (while $M_{\theta}/M_{\phi} = \text{constant}$); (b) the ratio of the phase-field and orientational mobilities (M_{θ}/M_{ϕ}), which is proportional to the ratio of the rotational and translational diffusion coefficients, ($M_{\theta}/M_{\phi} \propto \chi = D_{\text{rot}}/D_{\text{trans}}$); and (c) the depth of the metastable free-energy well for branching. The physical background of these processes in enhancing GFN is as follows. (a) Increasing the thermodynamic driving force accelerates crystal growth, thus decreasing the time available for orientational ordering. In turn, this leads to the formation of groups of dislocations comprising orientational defects that can serve as a source of newly oriented domains at the interface. (b) Decreasing the magnitude of the orientational mobility relative to the phase-field mobility again decreases the time available for orientational ordering, leading to the formation of orientational defects. (c) Increasing the depth of the free-energy well for branching increases the probability of branching events, which again increases the rate of formation of new orientations. Any of these processes or any combination thereof can drive the system to form crystal sheaves and eventually spherulites.

Indeed, by varying any of these parameters, the solidification morphology can be tuned between a single needle crystal and a spherulite, as demonstrated for mechanism (iii) in Fig. 4. Analogous changes can be obtained for mechanism (ii) in cases (a) and (b). To a first approximation, in all cases, the final ($t \rightarrow \infty$) volume fraction of the crystalline phase is determined via the lever rule by the initial degree of supersaturation $S = (c_0 - c_s)/(c_L - c_s)$. Here, c_0 , c_s , and c_L are the initial, solidus, and liquidus compositions, respectively; S is approximately constant for cases (b) and (c).

As our phase-field model relies on a coarse-grained-order parameter to monitor crystallization, microscopic details such as crystal structure and molecular geometry are reflected only in the anisotropies of the interfacial free energies and mobilities, which the model receives as input. A small number of such model parameters is sufficient to simulate many experimental morphologies [23, 24, 26, 28], some of which have been observed in systems of very different molecular natures. This, together with the observation that similar morphologies evolve in systems of different molecular

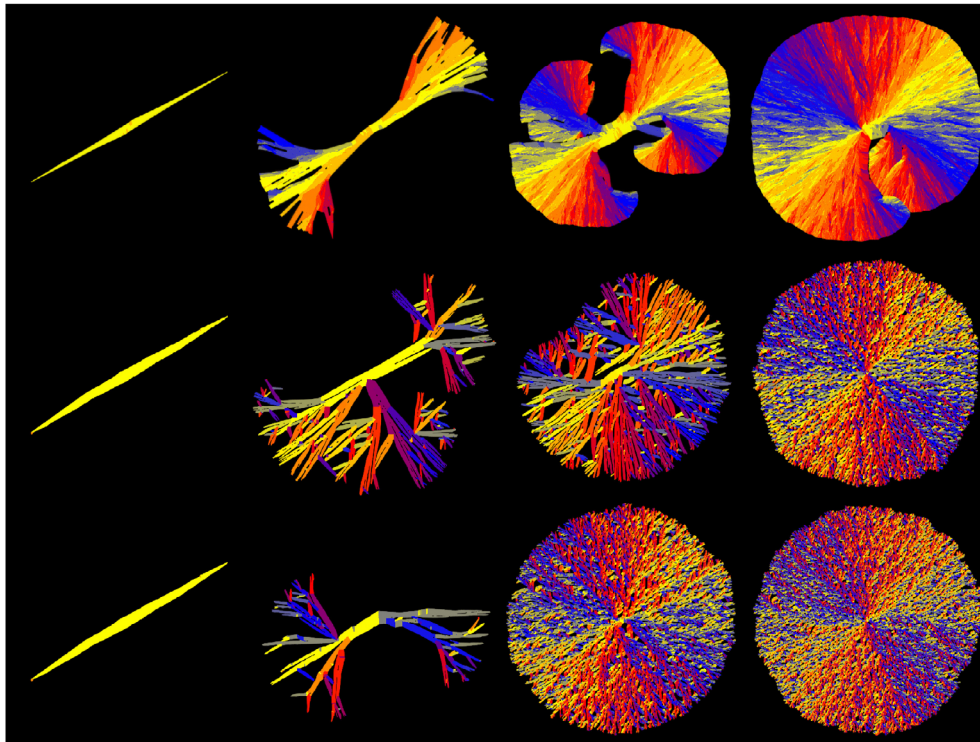


Figure 4 Three growth paths from needle crystals to polycrystalline spherulites: the effect of parameters governing GFN in phase-field theory in the case of mechanism (iii) (branching with fixed crystallographic misorientation). Upper row: The thermodynamic driving force of crystallization is varied, monitored by the degree of supersaturation ($S = 0.70, 1.0, 1.15,$ and 1.20 ; $x = 0.25$; $M_\theta/M_\phi = \chi = 60.51$; branching angle: 15°). To model the morphologies of PNT aggregates more closely, in addition to the anisotropy of the phase-field mobility, we have incorporated a four-fold anisotropy for the interfacial free energy via the coefficient of the square-gradient term, as specified in Refs. [23, 25, 26, 28]. Central row: The ratio of the orientational and phase-field mobilities is varied ($M_\theta/M_\phi = 0.2\chi, 0.125\chi, 0.1\chi,$ and 0.05χ ; $S = 0.95$; $x = 0.1$, branching angle 30°). Bottom row: The depth of the metastable well in the orientation free energy f_{ori} is varied ($x = 0.1, 0.15, 0.175,$ and 0.2 ; $S = 0.95$; $M_\theta/M_\phi = 0.2\chi$, branching angle 30°). The simulations are performed on a $2,000 \times 2,000$ grid. The early stages of solidification are shown, in which the growth morphologies are clearly seen. The late-stage (equilibrium) crystalline fraction is determined by the degree of supersaturation via the lever rule, and thus changes only in the upper row.

geometry, suggests that these coarse-grained-model parameters may be responsible for the formation of similar structures in microscopically and chemically dissimilar systems, and thus can be useful in understanding the origin of the observed morphologies.

While for monatomic systems, the interfacial free energies, mobilities, and anisotropies can be obtained from atomistic simulations [29] that enable quantitative phase-field modeling; this has not yet been achieved for complex systems such as polymers or PNTs. Therefore, we perform the simulations for a model material used in previous studies [23, 24, 26, 28, 30]. The magnitude of the anisotropy of the interfacial free energy and kinetic coefficient, the branching angle, and the activation energy of branching are not known.

However, some qualitative features may be guessed. The highly anisotropic growth of the needle-crystal morphology observed in systems with lower driving forces indicates a strong two-fold anisotropy for the kinetic coefficient (i.e., the phase-field mobility); the faceted shapes, observed at high magnification for the needle crystals, imply a highly anisotropic interfacial free energy.

2.3 Discussion

Earlier observations demonstrated that humidity is important to various self-assembly processes. Among many examples, apparent humidity effects have been observed in the cases of the adhesion of vertically aligned carbon NT films [31] and the mobility of

organic monolayers when creating aggregate islands [5]. To this point, temperature and chemical composition were considered the dominant parameters controlling solidification [1, 5]. In the present experiments, the temperature was steadily maintained with high accuracy.

The driving force for the self-assembly of nano-size objects is the difference in grand potential between the liquid and solid phases, which can be obtained from a thermodynamic assessment of the PNT-NMP-water system. The grand potential relates to the local composition of the fluid and the phase diagram of the ternary system. In principle, it could be obtained from literature data [31, 32], once the local composition is known. The humidity of the air may be crucial to phase-separation dynamics. For example, in vapor-induced phase separation (VIPS) [31, 32], where the initial casting solution contains both solvent and polymer, increasing the relative humidity increases the driving force for the net diffusion of water into the film and water accumulation in it, thereby inducing phase separation. The critical humidity for the accumulation of water in many systems containing both NMP and water is ~60%, as in the results reported here. Accordingly, humidity has a significant influence on the phase-transformation kinetics and the final morphology in VIPS [32, 33].

Although the initial chemical composition of the fluid layer has been well defined, the water content is expected to vary with time as a result of water adsorption from the air and water diffusion from the free surface of the sample inside the fluid layer, as previously modeled and discussed [33]. This change in the overall composition of the liquid layer from which the PNT aggregate precipitates should depend on the controlled humidity of the laboratory, and is expected to change the driving force for PNT aggregation [33]. In turn, this change should be reflected in the volume fraction of the crystalline phase of the aggregate. Indeed, in the observed solidification morphologies, a clear correlation with the actual humidity is found (see Figs. 2 and 3) that also manifests in the change of the final crystalline fraction X (X is proportional to the surface coverage, which increases with increasing humidity, as evident from the experimental images; see Fig. 2(b)). In

addition to the driving force for aggregation, the changing water content can influence the orientational and translational diffusion coefficients, by affecting the viscosity η of the fluid. However, at the small degrees of undercooling used here, both the translational and rotational diffusion coefficients scale with $1/\eta$; this effect is expected to cancel to a first approximation. This leaves the interpretation of the observed morphological transformations as consequences of the changes in the thermodynamic driving force for PNT aggregation, resulting from the incorporation of water into the fluid phase from the humid air environment. In principle, the water content could also influence the energetics of branching via adsorption at the solid-liquid and solid-solid interfaces; however, the direction of this effect is unclear. Furthermore, this mechanism does not explain the observed change in the final volume fraction of the crystalline phase, which indicates a change in the driving force.

In a previous work, it was found that the presence of NMP increased the metastable zone width of nitrotriazolone (NTO)–water systems [32, 33]. The rapid deposition of the solute and the high production rate of nuclei enabled the formation of smooth-surfaced spherulitic crystals. Humidity appeared to have the double roles of water sorption and solubility changes in the ternary phase diagram for this system. It was previously found that the growth rate of the solid phase increased with increasing water content of the co-solvent [32, 33]. These findings suggested that the metastable zone width could be controlled by adjusting the ratio of water–NMP, which was coupled to the humidity of the atmosphere. Hence, we expect that the change in driving force (case (a), discussed above and illustrated by the first row of Fig. 4) is responsible for the observed morphological transition from needle crystals to spherulites of the PNT aggregates in this system.

Finally, while the two homogeneous mechanisms (ii) and (iii) of GFN lead to similar morphologies, the distributions of the orientation of the crystal grains composing a single spherulite differ for the two mechanisms. This can be verified by performing a statistical analysis of the spherulitic orientations. While quantitative analyses can be performed in the simulations (see ESM), we are limited to a qualitative

analysis based on visual inspection in the experimental case. This mainly arises from the soft-matter used, the inhomogeneity of the sample, the degree of crystallinity, and the surface roughness (see ESM for a qualitative analysis). Nevertheless, according to previous studies, the change of humidity certainly influences the thermodynamic driving force of crystallization, which may solely have caused the observed morphological transitions in the spherulitic formations, according to the phase-field simulations. Humidity appears to be an essential governing parameter of the evolution of the morphology, which is often overlooked.

3 Summary

We have demonstrated that humidity can be used to control the growth of MHSA PNT aggregates, yielding various growth morphologies. The PNT-solvent system serves as an excellent test bed for exploring general trends in morphology selection. A general phase-field model of polycrystalline freezing, proposed recently to describe GFN, was used to explore the physical basis of the observed morphological transitions. The GFN mechanisms are identified as variations of the driving force of crystallization resulting from changes in the water content via adsorption from the atmosphere. Based on the close similarity between the experimental results and the computer simulations, we expect that the development of a humidity-controlled methodology is feasible. This method would harness the manipulation of GFN mechanisms to tailor the morphology of spherulites for a range of practical applications.

Acknowledgements

This work has been supported by the Israel Science Foundation (No. 434/12) and by the National Agency for Research, Development, and Innovation, Hungary under contract OTKA-K-115959.

Electronic Supplementary Material: Supplementary material (structure of spherulites: phase-field modelling, structure of PNT spherulites: experiments, preparation of PNT samples) is available in the online version of

this article at <http://dx.doi.org/10.1007/s12274-015-0863-2>.

References

- [1] Mann, S. Self-assembly and transformation of hybrid nano-objects and nanostructures under equilibrium and non-equilibrium conditions. *Nat. Mater.* **2009**, *8*, 781–792.
- [2] O’Leary, L. E. R.; Fallas, J. A.; Bakota, E. L.; Kang, M. K.; Hartgerink, J. D. Multi-hierarchical self-assembly of a collagen mimetic peptide from triple helix to nanofibre and hydrogel. *Nat. Chem.* **2011**, *3*, 821–828.
- [3] Mirkin, C. A.; Letsinger, R. L.; Mucic, R. C.; Storhoff, J. J. A DNA-based method for rationally assembling nanoparticles into macroscopic materials. *Nature* **1996**, *382*, 607–609.
- [4] Schlittler, R. R.; Seo, J. W.; Gimzewski, J. K.; Durkan, C.; Saifullah, M. S. M.; Welland, M. E. Single crystals of single-walled carbon nanotubes formed by self-assembly. *Science* **2001**, *292*, 1136–1139.
- [5] Harada, A.; Kobayashi, R.; Takashima, Y.; Hashidzume, A.; Yamaguchi, H. Macroscopic self-assembly through molecular recognition. *Nat. Chem.* **2011**, *3*, 34–37.
- [6] Adler-Abramovich, L.; Aronov, D.; Beker, P.; Yevnin, M.; Stempler, S.; Buzhansky, L.; Rosenman, G.; Gazit, E. Self-assembled arrays of peptide nanotubes by vapour deposition. *Nat. Nanotechnol.* **2009**, *4*, 849–854.
- [7] Whitesides, G. M.; Grzybowski, B. Self-assembly at all scales. *Science* **2002**, *295*, 2418–2421.
- [8] Hendler, N.; Sidelman, N.; Reches, M.; Gazit, E.; Rosenberg, Y.; Richter, S. Formation of well-organized self-assembled films from peptide nanotubes. *Adv. Mater.* **2007**, *19*, 1485–1488.
- [9] Reches, M.; Gazit, E. Controlled patterning of aligned self-assembled peptide nanotubes. *Nat. Nanotechnol.* **2006**, *1*, 195–200.
- [10] Sidelman, N.; Rosenberg, Y.; Richter, S. Peptide-based spherulitic films-formation and properties. *J. Colloid Interface Sci.* **2010**, *343*, 387–391.
- [11] Magill, J. H. Review spherulites: A personal perspective. *J. Mater. Sci.* **2001**, *36*, 3143–3164.
- [12] Ryschenkow, G.; Faivre, G. Bulk crystallization of liquid selenium Primary nucleation, growth kinetics and modes of crystallization. *J. Cryst. Growth* **1988**, *87*, 221–235.
- [13] James, P. F. In *Advances in Ceramics*; Uhlman, D. R.; Beagle, G. H.; Simmons, J. H., Eds.; American Ceramic Society: Columbus, Ohio, 1982; Vol. 4, pp 1–48.
- [14] Köster, U.; Herold, U. Crystallization of metallic glasses. In *Glassy Metals I*; Güntherodt, J. H.; Beck, H., Eds.; Springer: Berlin, Heidelberg, 1981; Vol. 46, pp 225–259.

- [15] Sperling, L. H. *Introduction to Physical Polymer Science*; Wiley: New York, 1992; Vol. 6.
- [16] Hutter, J. L.; Bechhoefer, J. Banded spherulitic growth in a liquid crystal. *J. Cryst. Growth* **2000**, *217*, 332–343.
- [17] Keith, H. D.; Padden, F. J. Jr. A phenomenological theory of spherulitic crystallization. *J. Appl. Phys.* **1963**, *34*, 2409–2421.
- [18] Walker, M. L.; Smith, A. P.; Karim, A., (unpublished).
- [19] Ojeda, J. R.; Martin, D. C. High-resolution microscopy of PMDA-ODA polyimide single crystals. *Macromolecules* **1993**, *26*, 6557–6565.
- [20] Geil, P. H. *Polymer Single Crystals*; Wiley: New York, 1963.
- [21] Hosier, I. L.; Bassett, D. C.; Vaughan, A. S. Spherulitic growth and cellulation in dilute blends of monodisperse longn-alkanes. *Macromolecules* **2000**, *33*, 8781–8790.
- [22] Khoury, F. The spherulitic crystallization of isotactic polypropylene from solution: On the evolution of monoclinic spherulites from dendritic chain-folded crystal precursors. *J. Res. Natl. Bur. Stand., Sect. A* **1996**, *70A*, 29–61.
- [23] Gránásy, L.; Pusztai, T.; Börzsönyi, T.; Warren, J. A.; Douglas, J. F. A general mechanism of polycrystalline growth. *Nat. Mater.* **2004**, *3*, 645–650.
- [24] Gránásy, L.; Pusztai, T.; Tegze, G.; Warren, J. A.; Douglas, J. F. Growth and form of spherulites. *Phys. Rev. E* **2005**, *72*, 011605.
- [25] Warren, J. A.; Boettinger, W. J. Prediction of dendritic growth and microsegregation patterns in a binary alloy using the phase-field method. *Acta Metall. Mater.* **1995**, *43*, 689–703.
- [26] Gránásy, L.; Börzsönyi, T.; Pusztai, T. Nucleation and bulk crystallization in binary phase field theory. *Phys. Rev. Lett.* **2002**, *88*, 206105.
- [27] Kobayashi, R.; Warren, J. A.; Carter, W. C. Vector-valued phase field model for crystallization and grain boundary formation. *Physica D* **1998**, *119*, 415–423.
- [28] Gránásy, L.; Pusztai, T.; Borzsönyi, T.; Warren, J. A.; Kvamme, B.; James, P. F. Nucleation and polycrystalline solidification in binary phase field theory. *Phys. Chem. Glasses* **2004**, *45*, 107–115.
- [29] Hoyt, J. J.; Asta, M.; Karma, A. Atomistic and continuum modeling of dendritic solidification. *Mat. Sci. Eng. R* **2003**, *41*, 121–163.
- [30] For specificity, we employ the well-studied, ideal solution phase diagram of the Ni-Cu alloy. This choice is not particularly restrictive, as it is formally equivalent to a pure material, where thermal diffusion replaces solute diffusion as the dominant transport mechanism. Moreover, the model is no way restricted to metals as our previous applications for polymers demonstrate. As in former studies, we fix the temperature to be 1,574 K. The orientation dependence of the molecular attachment kinetics is modelled by $M_\phi = M_{\phi_0} \{1 + \delta_0 \cos[k(\psi - \theta)]\}$. The angle ψ is the inclination of the liquid-solid interface in the laboratory frame and k is the symmetry index. The fibre-like crystallites forming in PNT matter imply a two-fold symmetry ($k = 2$) and a large kinetic anisotropy, which was chosen as $\delta_0 = 0.995$. A similar approach is used to describe the anisotropy of the interfacial free energy: $\gamma = \gamma_0 \{1 + s_0 \cos[k(\psi - \theta)]\}$. Crystal growth is sensitive to both of these anisotropies; increasing either of them yields sharper needle crystal morphologies. Our computations were performed with supersaturations in the range $0.7 \leq S = (c_L - c)/(c_L - c_S) \leq 1.2$, where c_L , c_S and c are the concentrations at the liquidus, solidus, and the initial homogeneous liquid mixture, respectively.
- [31] Zhang, Z. J.; Wei, B.; Ward, J. W.; Vajtai, R.; Ramanath, G.; Ajayan, P. M. Select pathways to carbon nanotube film growth. *Adv. Mater.* **2001**, *13*, 1767–1770.
- [32] Kim, K. J.; Kim, K. M. Growth kinetics in seeded cooling crystallization of 3-nitro-1,2,4-triazol-5-one in water-N-methylpyrrolidone. *Powder Technol.* **2002**, *122*, 46–53.
- [33] Yip, Y.; McHugh, A. J. Modeling and simulation of nonsolvent vapor-induced phase separation. *J. Membrane Sci.* **2006**, *271*, 163–176.